Bio-Inspired Dual-Auger Vertical Self-Burrowing Robot: DEM-MBD Analysis of Downward Penetration in Granular Media

Preprint · May 2024

DOI: 10.13140/RG.2.2.32849.54885

Sarina Shahhosseini

Arizona State University

Bio-Inspired Dual-Auger Vertical Self-Burrowing Robot: DEM-MBD Analysis of Downward Penetration in Granular Media

Sarina Shahhosseini, S.M.ASCE[1] and Junliang Tao, Ph.D., A.M.ASCE[2,*]

[1]Graduate Student, School of Sustainable Engineering and the Built Environment, Center for Bio-mediated and Bio-inspired Geotechnics, Arizona State University, 650 E Tyler Mall, Tempe, AZ 85281 Email: sshahho1@asu.edu
[2]Associate Professor, School of Sustainable Engineering and the Built Environment, Center for Bio-mediated and Bio-inspired Geotechnics, Arizona State University, 650 E Tyler Mall, Tempe, AZ 85287 Email: jtao25@asu.edu
[*]Corresponding author

ABSTRACT

Geotechnical engineering is crucial for infrastructure development, requiring precise subsurface investigation. Traditional penetration methods face increased difficulties and costs as effective stress rises with depth. In this paper, we present a bio-inspired robot capable of downward self-burrowing in granular media, drawing from nature's adaptive strategies in subterranean environments. We applied a coupled discrete element method (DEM) and multi-body dynamics (MBD) framework to analyze the self-burrowing behavior of the robot in dry sand. Using Project Chrono, an open-source physics engine, we integrated DEM for detailed soil-robot interaction modeling and MBD for the robot's dynamic response.

The robot, inspired by awned seeds, features dual vertically aligned auger-shaped bodies connected to rotational motors, incorporating both contraction and extension mechanisms. Simulated in a packing of monodisperse frictional spheres, the interaction between the robot and sand is modeled with high fidelity. Our analysis focused on two operational cycles: Cycle 1 involves the rotation of the upper auger and contraction of the linear actuator, generating downward thrust. Cycle 2 involves the rotation of the lower auger and extension of the linear actuator, also generating downward thrust. Results indicate that the respective augers provide thrust during their active cycles and act as anchors during the other cycle. The robot's downward movement depends significantly on its initial embedment depth, with both upper and lower parts providing essential anchorage. At greater depths, the resistive forces and thrust forces increase, improving the robot's burrowing efficiency. Future work will identify the breaking points for optimal self-burrowing and further optimize the robot's design for various soil conditions.

INTRODUCTION

In recent years, strategies inspired by nature have gained traction in geotechnics, offering efficient and multifunctional solutions to engineering problems (Zhang et al. 2023, 2024). The biological world, with its diverse range of materials and mechanical systems, provides a wealth of ideas that can be abstracted and adapted to solve engineering challenges (Martinez et al. 2022). Meanwhile, robotic techniques have revolutionized various industries and aspects of daily life by freeing the human labor force, enhancing industrial processes, automating repetitive tasks, and operating in hazardous environments where humans struggle to survive (Chen et al. 2023). Despite these advancements, mobile robots have yet to achieve efficiency and success in subterranean environments due to the complexities of navigating terrestrial substrates (Aguilar et al. 2016; Treers et al. 2022). Understanding and overcoming these challenges are critical as we continue to push the boundaries of robotic applications on land, sea, and in space (Zhang and Goldman 2014).

Amid these advancements, bio-inspired geotechnics has emerged as a promising field. Innovations such as snakeskin-inspired surfaces (O'Hara and Martinez 2022), root-inspired anchorage systems (Mallett et al. 2021), and robotic excavation techniques are gaining attention. A new generation of burrowing robots, inspired by biological mechanisms like those of razor clams (Winter et al. 2014). is being developed to tackle geotechnical challenges (Shahhosseini et al. 2022; Tang and Julian Tao 2021; Tao et al. 2020). These robots are not only designed for site investigations (Martinez et al. 2019), but also for surveillance and sensor deployment (Martinez et al. 2022). By mimicking the efficient burrowing strategies found in nature, these bio-inspired robots hold the potential to revolutionize how we approach and solve problems in geotechnical engineering.

Previous work demonstrated the effectiveness of a dual-auger self-burrowing robot for horizontal penetration (Shahhosseini et al. 2022). Since geotechnical challenges often involve vertical penetration, our design focuses on a vertically self-burrowing robot. This robot's design and functionality comprise two main features: 1) a helical design with oscillatory motion, and 2) contraction/extension mechanisms. Drawing inspiration from nature, we looked at Erodium cicutarium seeds, which penetrate the soil through a winding and unwinding motion (Bagheri et al. 2024; Stamp 1984) , and razor clams, which enhance upward anchorage to reduce resistance during downward burrowing (Chen et al. 2021; Huang and Tao 2020; Huh et al. 2023). Our robot incorporates these bio-inspired mechanisms with two rotating augers to enhance downward thrust force and anchorage at each cycle .

The scallop theorem (Purcell 1997) posits that reciprocal motion in low Reynolds number fluid does not result in net movement, requiring an agent to alter its geometry or trajectory to achieve locomotion. In granular media, where drag forces dominate, this principle remains valid but involves additional complexity due to asymmetric material properties and changes in stress states or packing (Treers et al. 2022). Unlike fluids, granular media generate upward resistive forces even during horizontal motions, often leading to net upward movement from reciprocal motions (Tao et al. 2020). Therefore, effective downward progress in granular media necessitates breaking geometric symmetry and overcoming material asymmetry. To address this, a contraction/extension feature was added to our robot design, enhancing thrust forces for penetration.

Simulations can be used to test the robot's design efficiency and rapidly modify and update the design to achieve the desired behavior. The Discrete Element Method (DEM) is one of the most common numerical methods used in geotechnical engineering for studying granular media behaviors, soil-structure interactions, and soil-soil interactions. However, using DEM for robot movements typically involves predefined kinematic simulations (Zhong and Tao 2023). To address this, we coupled Multi-Body Dynamics (MBD) with DEM to analyze the robot's movement in a dynamic system, which is crucial for self-burrowing behavior. Project Chrono, an open-source physics-based platform, enables DEM-MBD simulation through its GPU module, expediting computationally expensive granular media simulations. In this project, we simulated a vertically self-burrowing bio-inspired robot using DEM-MBD and studied the effect of initial embedment depth on its behavior.

METHODOLAGY

Numerical Method and Set up. To simulate the robot's self-burrowing behavior, we utilized the DEM-MBD numerical method to analyze robot-particle interactions. We primarily used Chrono::Engine and Chrono::GPU from Project Chrono, an open-source physics-based engine (Mazhar et al. 2013). The robotic parts were defined as rigid bodies, with each body designed as an object with specified mesh geometries. In DEM-MBD co-simulation, the robotic body parts are connected via links (rotational and linear motors) to create a dynamic system. The co-simulation process begins with the Chrono::GPU engine, which uses the DEM numerical model to compute contact forces, frictional tangential forces, rolling friction torque, and cohesion forces between the particles and the robot's surface. An application programming interface (API) facilitates the interaction between Chrono::GPU and the core engine. Finally, the kinematic updates in rigid robotic bodies are calculated based on the forces and torques computed in the previous step by applying MBD (Fang et al. 2021).

The particles in the simulation are modeled as spheres with a 3 mm diameter to mimic dry glass beads, representing dry sand. The particle and interaction properties are based on previous studies (Shahhosseini et al. 2022; Thoesen et al. 2019). The robot is simulated by connecting the rigid bodies via motors and links and then placing it in the particle setup.

To study the effect of initial embedment depth on the robot's self-burrowing behavior, we constructed the particle settlement in two phases. Phase one involves the initial particle settlement and placement of the robot at three different depths. Phase two starts when the robot begins its movement after complete settlement. In phase one, particles are layered using a disk sampling method and allowed to settle and fall for 4 seconds resulting in 1018091 particles. To increase the density of the sample, the particle-particle and particle-mesh friction coefficients in phase one are set to half of those in phase two. The setup is allowed to settle for an additional 2 seconds between these two phases to eliminate any unsettled particles. Phase one is conducted in three cases where the initial position of the robot varies, resulting in three different initial embedment depths after total settlement.

In case 1 of phase one, the center of the robot is placed 20 cm above the top layer of particles and then allowed to settle and fall with the particles. In case 2, the robot, placed in the same position, falls 1 second after the particles to allow for initial settlement. In case 3, the particles settle first, and then the robot falls from the same position. These three cases result in different embedment depths: case 1 results in a 24.5 cm embedment depth from the bottom tip of the robot; case 2 results in a 16.5 cm embedment depth; and case 3 results in a 6 cm embedment depth, where about 60% of the robot is not embedded in the granular media. Figure 1 shows the three cases.

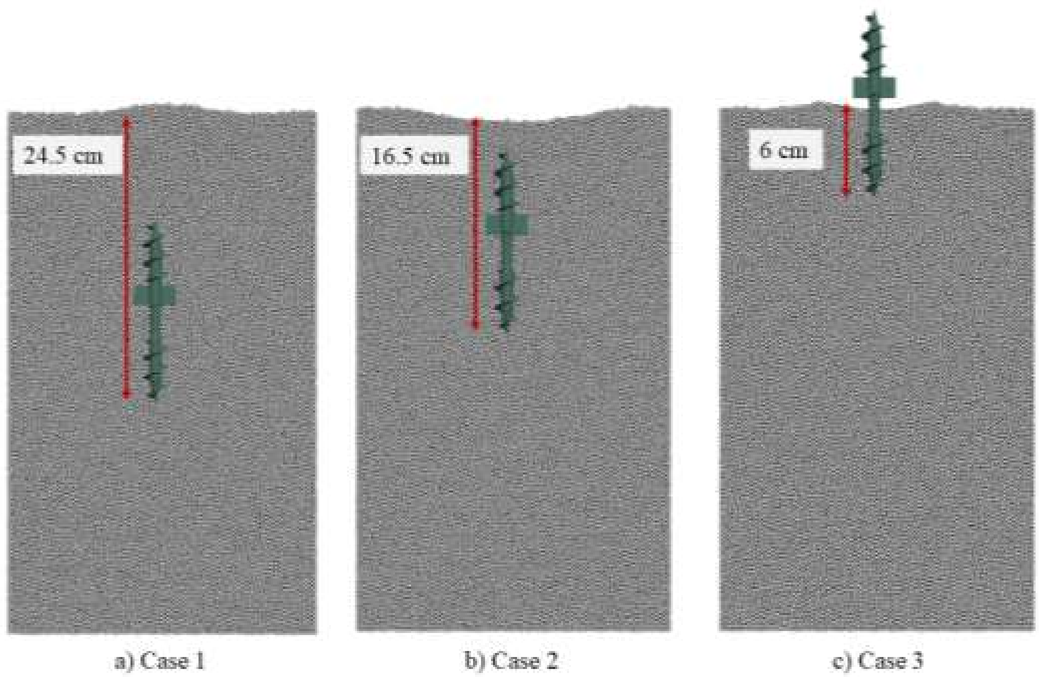

Figure 1: Initial embedment depths of the self-burrowing robot in three cases. (a) Case 1: Robot placed 20 cm above particles, resulting in a 24.5 cm embedment depth. (b) Case 2: Robot falls 1 second after particles, resulting in a 16.5 cm embedment depth. (c) Case 3: Robot placed after particles settle, resulting in a 6 cm embedment depth, with 60% of the robot unembedded.

Robot's Design and Mechanic of Movement. The robot consists of two identical augers positioned at the top and bottom, with two stators located in the middle. Each auger is connected to a stator via rotational motor links, while the two stators are linked by a linear actuator, resulting in a total of three motors. The upper stator has four blades to provide additional torque during the burrowing process (Shahhosseini et al. 2023). The detailed dimensions of the robot's components are shown in Figure *2*.

When starting the simulation, the robot's auger is in its extended position. The robot's movement mechanism is divided into two cycles.

Cycle 1: The upper auger rotates clockwise with 60 RPM to generate thrust forces, while the linear actuator between the two stators contracts with speed of 4cm/sec. This contraction generates additional thrust forces as the lower auger acts as an anchor by engaging its blades with the particles.

Cycle 2: While the upper auger remains stationary, the lower auger rotates at 60 RPM clockwise, and the lower stator extends at a speed of 4 cm/sec. In this cycle, the lower auger generates thrust forces, and the upper auger and stator act as the anchor.

The simulation runs for a total of 6 seconds, with each cycle lasting 1 second, allowing for three complete cycles. The robot's movement cycles are shown in Figure 3

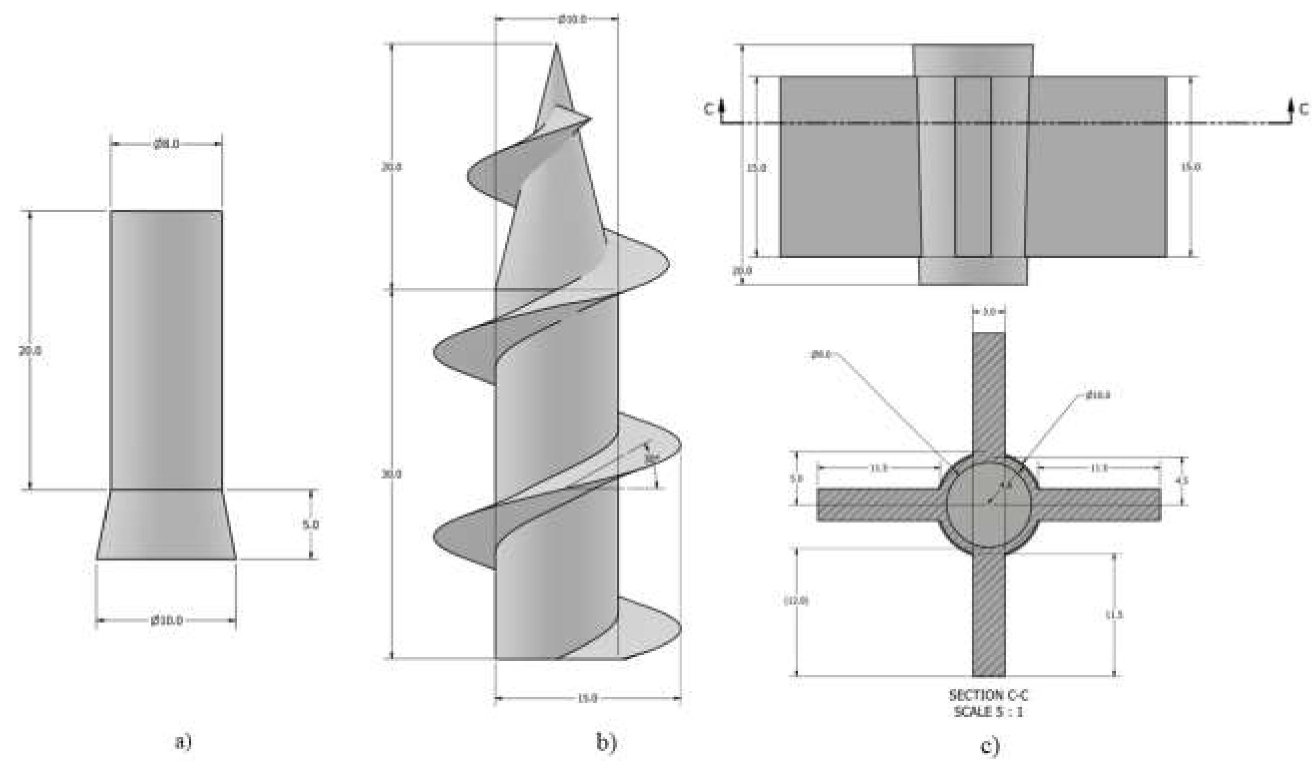

Figure 2: Detailed dimensions of the robot's components. (a) Lower stator dimensions, (b) Auger dimensions, and (c) Cross-sectional view of the upper stator, showing the arrangement of the blades and connections. All dimensions are in centimeters.

RESULTS:

Figure 4 shows the vertical displacement of the upper and lower augers, representing the displacement of the top and bottom of the robot. At an embedment depth of 6 cm, we can see that the lower auger does not move when the upper auger contracts and extends. In this case, during cycle 2, the upper auger and stator are not embedded and interacting with particles; hence, they do not provide additional anchorage.

For embedment depths of 24.5 cm and 16.5 cm, during cycle 1, when the upper auger rotates and the stator contracts, the upper part of the robot penetrates downward, while the lower auger and stator slightly move up, resulting in an upward slip. This is also showcased in Figure 3. The slip is less at higher depths as the lower auger provides greater anchorage. As the robot moves further down, the difference in the bottom part slip decreases.

Additionally, during cycle 2, when the lower auger is rotating and the linear actuator extends, the lower part of the robot penetrates and the upper part of the robot (upper auger and stator) slightly moves down, resulting in a downward slip. Interestingly, the slip seems to be greater for the 24.5 cm depth than for the 16.5 cm depth. At greater depths, not only does the upper part provide enough anchorage to prevent upward slip, but the lower auger also generates enough thrust force to push the upper part down.

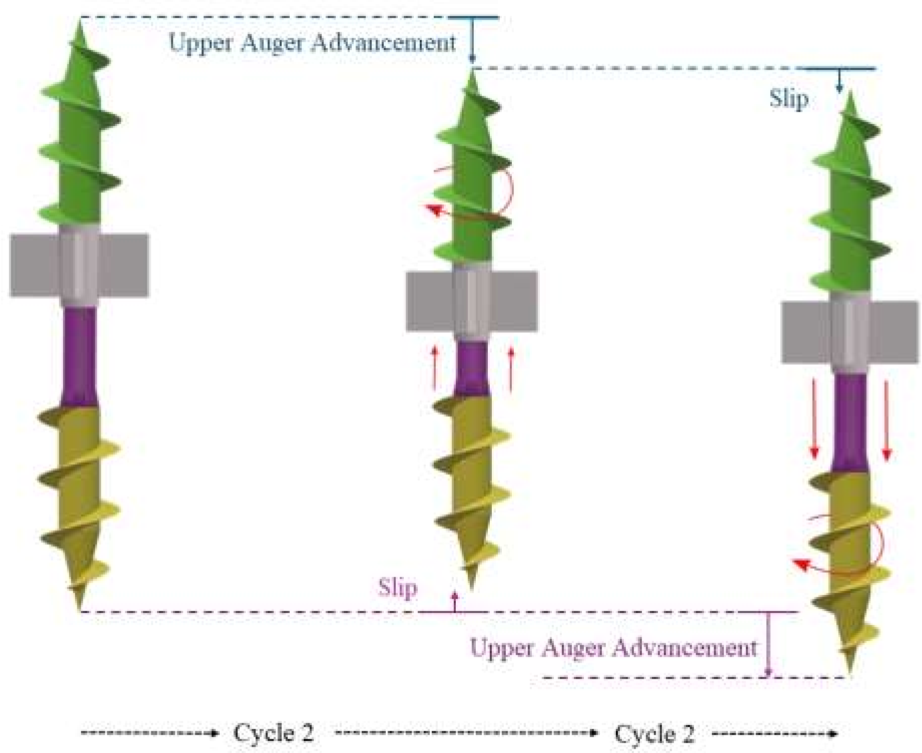

Figure 3: Movement cycles of the self-burrowing robot. (1) The upper auger rotates and contracts, with the lower auger anchoring. (2) The lower auger rotates and extends, with the upper auger anchoring.

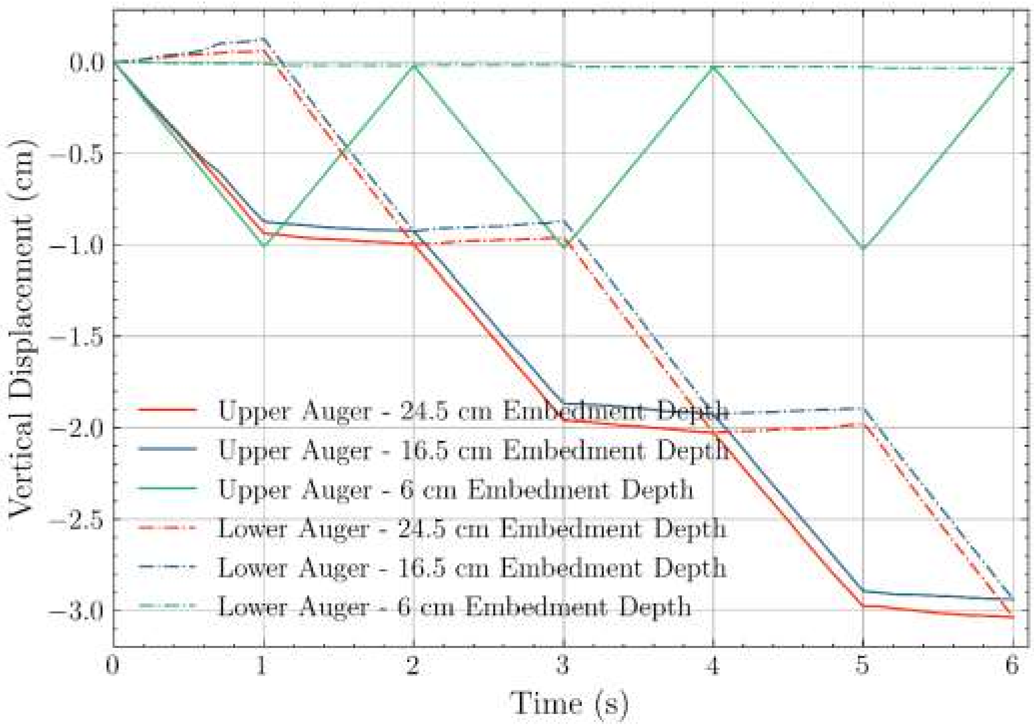

Figure 4: Vertical displacement over time for upper and lower augers at different embedment depths (24.5 cm, 16.5 cm, and 6 cm).

Comparing the embedment depths of 16.5 cm and 24.5 cm, where the robot is completely embedded, we see that the displacement in each cycle is 0.9 cm for 24.5 cm and 0.8 cm for 16.5 cm. This indicates that as we increase the embedment depth from not completely embedded to greater depth, the self-burrowing downward displacement of the robot increases from zero net displacement to 3.1 cm at 6 seconds.

Figure *5* and **Figure *6*** show the vertical forces applied by particles to the robot body parts. **Figure *5*** presents the forces on the upper auger and upper stator. The gray sections indicate the contraction cycles, where these parts are actively generating movement. Similarly, **Figure *6*** displays the vertical forces on the lower auger and stator, with the gray sections representing the extension cycles where these parts drive the robot's movement.

As the robot starts its movement with cycle 1 in contraction, the upper auger and stator move downward (**Figure *4***). In **Figure *5***, during the contraction cycle (gray section: Cycle 1), which shows the vertical forces on the upper body parts, the upper stator faces resistance, and the upper auger generates thrust in the downward direction. During the extension cycle (when the lower parts are active), there is a reduction in forces for both upper parts, indicating a change in force direction for the upper auger and a reduction in force magnitude for the upper stator. When extending, the upper parts act as anchorage, providing a downward force opposite to their expected upward movement. This anchorage force, seen as a reduction in the forces during the extension cycle, prevents upward movement. The upper stator experiences a reduction in vertical forces of about 2.5 N, and the upper auger experiences a change in force direction from negative to positive forces. Without this anchorage force, the upper parts would move upward, resulting in negative force values for both the upper stator and auger.

In cycle 2 at depths of 16.5 and 24.5 cm, the lower auger and stator are active and move downward (**Figure *4***). The forces on the lower parts in cycle 2, as shown in **Figure *6*** during the gray sections (Cycle 2: extension), indicate that the lower stator resists downward movement and the lower auger generates thrust, as the force from the particles applied to the auger is downward (negative). When it is not the extension cycle (white section: Cycle 1 during contraction), both the lower stator and auger act as anchorage, facing a reduction in thrust forces. The lower auger shows a decrease in negative thrust force, and the lower stator experiences negative forces as it resists upward movement during contraction. During this phase, the lower auger and stator do not move significantly (**Figure *4***). This occurs because granular media tend to create upward resistive forces on an intruder, and purely reciprocal motions often result in net upward movement (Tao et al., 2020).

For all body parts, the resistive forces during cycles 1 and 2 increase with depth. In cycle 1, the resistive force exerted by the upper stator at a depth of 24.5 cm increases from 4 N to 6 N over 6 seconds. During contraction, the lower auger generates considerable thrust force at depths of 24.5 cm and 16.5 cm, with the force increasing from about -1.5 N to -3 N over three cycles.

CONCLUSION:

In this paper, we used a DEM-MBD framework to analyze the downward self-burrowing movements of a bio-inspired robot with rotational and contraction/extension mechanisms in two cycles. The robot was placed at three different depths to study the effect of initial embedment depth on its movements. The results indicate that the downward movements of the robot depend significantly on its initial depth, and it is imperative that the robot is fully positioned in the soil so both the upper and lower parts provide anchorage. Our findings show that during their respective cycles, the stators experience resistive forces while the augers generate thrust forces. When not in their active cycle (upper stator and auger in cycle 2, and lower stator and auger in cycle 1), the parts act as anchorage to prevent upward movement of the robot. It was observed that the thrust forces generated by the lower auger are greater than those generated by the upper auger due to the increased stress forces faced by the granular media at greater depths.

Future work will focus on identifying the breaking points at which the robot will self-burrow more effectively. Additionally, further research will explore optimizing the robot's design to enhance its self-burrowing capabilities in various soil conditions.

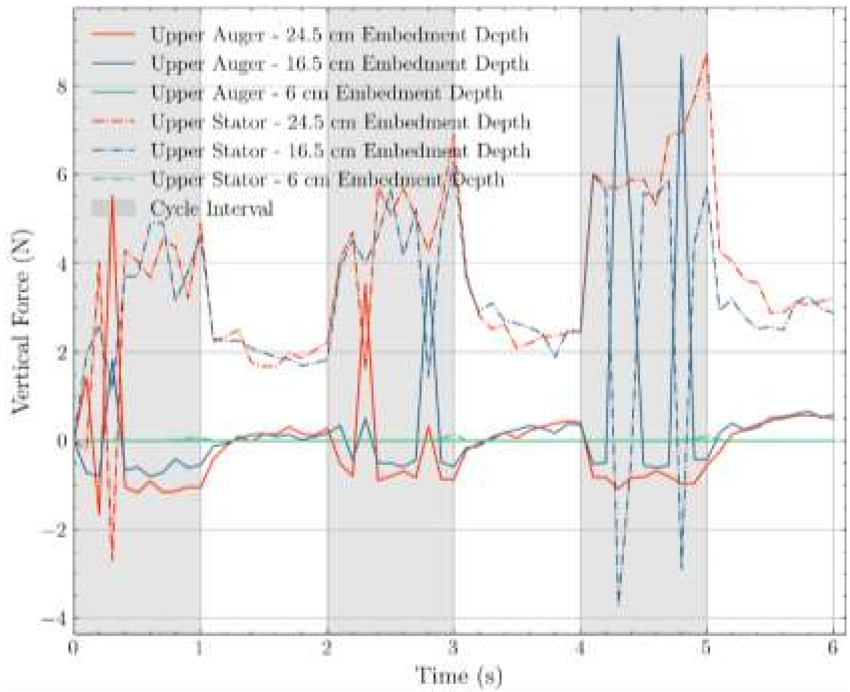

Figure 5: Vertical forces on the Upper auger and stator over time for different embedment depths. Gray sections indicate extension cycles : cycle 1) where these parts are active.

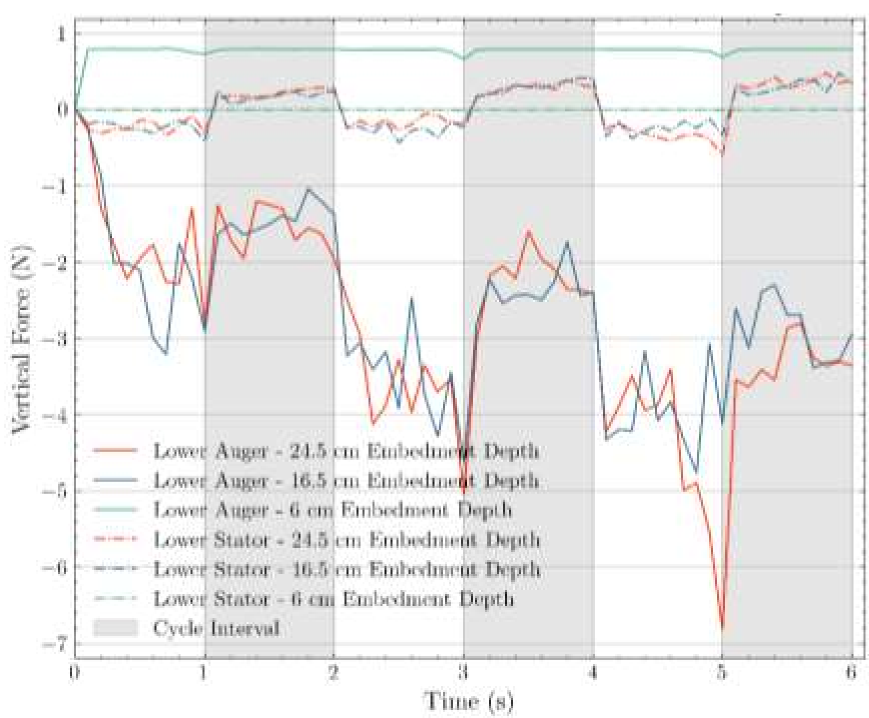

Figure 6:Vertical forces on the lower auger and stator over time for different embedment depths. Gray sections indicate contraction cycles : cycle 2) where these parts are active.

ACKNOWLEDGEMENT

This material is based upon work supported by the National Science Foundation (NSF) under NSF CMMI 1849674 and CMMI 1841574. Any opinions, findings, and conclusions or recommendations expressed in this material are those of the authors and do not necessarily reflect those of the NSF.

REFRENCES

Aguilar, J., T. Zhang, F. Qian, M. Kingsbury, B. McInroe, N. Mazouchova, C. Li, R. Maladen, C. Gong, M. Travers, R. L. Hatton, H. Choset, P. B. Umbanhowar, and D. I. Goldman. 2016. "A review on locomotion robophysics: the study of movement at the intersection of robotics, soft matter and dynamical systems." *Rep. Prog. Phys.*, 79 (11): 110001. IOP Publishing. https://doi.org/10.1088/0034-4885/79/11/110001.

Bagheri, H., D. Stockwell, B. Bethke, N. K. Okwae, D. Aukes, J. Tao, and H. Marvi. 2024. "A bio-inspired helically driven self-burrowing robot." *Acta Geotech.*, 19 (3): 1435–1448. https://doi.org/10.1007/s11440-023-01882-9.

Chen, Y., A. Khosravi, A. Martinez, and J. DeJong. 2021. "Modeling the self-penetration process of a bio-inspired probe in granular soils." *Bioinspir. Biomim.*, 16 (4): 046012. IOP Publishing. https://doi.org/10.1088/1748-3190/abf46e.

Chen, Y., Y. Zhang, H. Li, J. Shen, F. Zhang, J. He, J. Lin, B. Wang, S. Niu, Z. Han, and Z. Guo. 2023. "Bioinspired hydrogel actuator for soft robotics: Opportunity and challenges." *Nano Today*, 49: 101764. https://doi.org/10.1016/j.nantod.2023.101764.

Fang, L., R. Zhang, C. Vanden Heuvel, R. Serban, and D. Negrut. 2021. "Chrono::GPU: An Open-Source Simulation Package for Granular Dynamics Using the Discrete Element Method." *Processes*, 9 (10): 1813. Multidisciplinary Digital Publishing Institute. https://doi.org/10.3390/pr9101813.

Huang, S., and J. Tao. 2020. "Modeling Clam-inspired Burrowing in Dry Sand using Cavity Expansion Theory and DEM." *Acta Geotech.*, 15 (8): 2305–2326. https://doi.org/10.1007/s11440-020-00918-8.

Huh, T. M., C. Cao, J. Aderibigbe, D. Moon, and H. S. Stuart. 2023. "Walk-Burrow-Tug: Legged Anchoring Analysis Using RFT-Based Granular Limit Surfaces." *IEEE Robotics and Automation Letters*, 8 (6): 3796–3803. https://doi.org/10.1109/LRA.2023.3269324.

Mallett, S. D., J. D. Frost, and J. A. Huntoon. 2021. "Root-Inspired Anchorage Systems for Uplift and Lateral Force Resistance." 299–307. American Society of Civil Engineers. https://doi.org/10.1061/9780784483411.029.

Martinez, A., J. Dejong, I. Akin, A. Aleali, C. Arson, J. Atkinson, P. Bandini, T. Baser, R. Borela, R. Boulanger, M. Burrall, Y. Chen, C. Collins, D. Cortes, S. Dai, T. DeJong, E. Del Dottore, K. Dorgan, R. Fragaszy, J. D. Frost, R. Full, M. Ghayoomi, D. I. Goldman, N. Gravish, I. L. Guzman, J. Hambleton, E. Hawkes, M. Helms, D. Hu, L. Huang, S. Huang, C. Hunt, D. Irschick, H. T. Lin, B. Lingwall, A. Marr, B. Mazzolai, B. McInroe, T. Murthy, K. O'Hara, M. Porter, S. Sadek, M. Sanchez, C. Santamarina, L. Shao, J. Sharp, H. Stuart, H. H. Stutz, A. Summers, J. Tao, M. Tolley, L. Treers, K. Turnbull, R. Valdes, L. van Paassen, G. Viggiani, D. Wilson, W. Wu, X. Yu, and J. Zheng. 2022. "Bio-inspired

geotechnical engineering: principles, current work, opportunities and challenges." *Géotechnique*, 72 (8): 687–705. ICE Publishing. https://doi.org/10.1680/jgeot.20.P.170.
Martinez, A., J. DeJong, R. Jaegar, and A. Khosravi. 2019. "Evaluation of self-penetration potential of a bio-inspired site characterization probe by cavity expansion analysis." *Canadian Geotechnical Journal*. http://dx.doi.org/10.1139/cgj-2018-0864.
Mazhar, H., T. Heyn, A. Pazouki, D. Melanz, A. Seidl, A. Bartholomew, A. Tasora, and D. Negrut. 2013. "CHRONO: A parallel multi-physics library for rigid-body, flexible-body, and fluid dynamics." *Mech. Sci.*, 4 (1): 49–64. https://doi.org/10.5194/ms-4-49-2013.
O'Hara, K. B., and A. Martinez. 2022. "Load Transfer Directionality of Snakeskin-Inspired Piles during Installation and Pullout in Sands." *Journal of Geotechnical and Geoenvironmental Engineering*, 148 (12): 04022110. American Society of Civil Engineers. https://doi.org/10.1061/(ASCE)GT.1943-5606.0002929.
Purcell, E. M. 1997. "The efficiency of propulsion by a rotating flagellum." *Proceedings of the National Academy of Sciences*, 94 (21): 11307–11311. https://doi.org/10.1073/pnas.94.21.11307.
Shahhosseini, S., M. Parekh, and J. Tao. 2022. "DEM-MBD Coupled Simulation of a Burrowing Robot in Dry Sand." *GeoCongress*.
Shahhosseini, S., M. Parekh, and J. Tao. 2023. "DEM-MBD Coupled Simulation of a Burrowing Robot in Dry Sand." 309–317. American Society of Civil Engineers. https://doi.org/10.1061/9780784484692.032.
Stamp, N. E. 1984. "Self-Burial Behaviour of Erodium Cicutarium Seeds." *Journal of Ecology*, 72 (2): 611–620. [Wiley, British Ecological Society]. https://doi.org/10.2307/2260070.
Tang, Y., and J. Julian Tao. 2021. "Effect of Rotation on Penetration: Toward a Seed Awn-Inspired Self-Burrowing Probe." *IFCEE 2021*, 149–159.
Tao, J. (Julian), S. Huang, and Y. Tang. 2020. "SBOR: a minimalistic soft self-burrowing-out robot inspired by razor clams." *Bioinspir. Biomim.*, 15 (5): 055003. IOP Publishing. https://doi.org/10.1088/1748-3190/ab8754.
Thoesen, A., T. McBryan, and H. Marvi. 2019. "Helically-driven granular mobility and gravity-variant scaling relations." *RSC Adv.*, 9 (22): 12572–12579. https://doi.org/10.1039/C9RA00399A.
Treers, L. K., B. McInroe, R. J. Full, and H. S. Stuart. 2022. "Mole crab-inspired vertical self-burrowing." *Front. Robot. AI*, 9. Frontiers. https://doi.org/10.3389/frobt.2022.999392.
Winter, A. G., V, R. L. H. Deits, D. S. Dorsch, A. H. Slocum, and A. E. Hosoi. 2014. "Razor clam to RoboClam: burrowing drag reduction mechanisms and their robotic adaptation." *Bioinspiration & Biomimetics*, 9 (3): 036009. https://doi.org/10.1088/1748-3182/9/3/036009.
Zhang, N., Y. Chen, A. Martinez, and R. Fuentes. 2023. "A Bioinspired Self-Burrowing Probe in Shallow Granular Materials." *Journal of Geotechnical and Geoenvironmental Engineering*, 149 (9): 04023073. American Society of Civil Engineers. https://doi.org/10.1061/JGGEFK.GTENG-11507.
Zhang, T., and D. I. Goldman. 2014. "The effectiveness of resistive force theory in granular locomotion." *Physics of Fluids*, 26 (10): 101308. https://doi.org/10.1063/1.4898629.
Zhang, W., R. Huang, J. Xiang, and N. Zhang. 2024. "Recent advances in bio-inspired geotechnics: From burrowing strategy to underground structures." *Gondwana Research*, 130: 1–17. https://doi.org/10.1016/j.gr.2023.12.018.

Zhong, Y., and J. (Julian) Tao. 2023. “Comparative Analysis of Horizontal Self-Burrowing Strategies Using Full-Scale DEM-MBD Co-Simulations.”